Published in final edited form as:
Toxicol Appl Pharmacol. 2012 August 15; 263(1): 81–88. doi:10.1016/j.taap.2012.06.001.

Phototoxicity of Nano Titanium Dioxides in HaCaT Keratinocytes – Generation of Reactive Oxygen Species and Cell Damage

Jun-Jie Yin[b,1], **Jun Liu**[a,1], **Marilyn Ehrenshaft**[c], **Joan E. Roberts**[d], **Peter P. Fu**[e], **Ronald P. Mason**[c], and **Baozhong Zhao**[a,*]

[a]CAS Key Laboratory for Biomedical Effects of Nanomaterials and Nanosafety, National Center for Nanoscience and Technology, Beijing 100190, China

[b]Center for Food Safety and Applied Nutrition, Food and Drug Administration, College Park, MD 20740, United States

[c]Laboratory of Toxicology and Pharmacology, National Institute of Environmental Health Sciences, NIH, Research Triangle Park, NC 27709, United States

[d]Fordham University, 113 West 60th Street, New York, NY 10023, United States

[e]National Center for Toxicological Research, Food and Drug Administration, Jefferson, AR 72079, United States

Abstract

Nano-sized titanium dioxide (TiO_2) is among the top five widely used nanomaterials for various applications. In this study, we determine the phototoxicity of TiO_2 nanoparticles (nano-TiO_2) with different molecular sizes and crystal forms (anatase and rutile) in human skin keratinocytes under UVA irradiation. Our results show that all nano-TiO_2 particles caused phototoxicity, as determined by the MTS assay and by cell membrane damage measured by the lactate dehydrogenase (LDH) assay, both of which were UVA dose- and nano-TiO_2 dose- dependent. The smaller the particle size of nano-TiO_2 the higher the cell damage. The rutile form of nano-TiO_2 showed less phototoxicity than anatase nano-TiO_2. The level of photocytotoxicity and cell membrane damage is mainly dependent on the level of reactive oxygen species (ROS) production. Using polyunsaturated lipids in plasma membranes and human serum albumin as model targets, and employing electron spin resonance (ESR) oximetry and immuno-spin trapping as unique probing methods, we demonstrated that UVA irradiation of nano-TiO_2 can induce significant cell damage, mediated by lipid and protein peroxidation. These overall results suggest that nano-TiO_2 is phototoxic to human skin keratinocytes, and that this phototoxicity is mediated by ROS generated during UVA irradiation.

*Address for correspondence and reprints: CAS Key Laboratory for Biomedical Effects of Nanomaterials and Nanosafety, National Center for Nanoscience and Technology, Beijing 100190, China Phone: +86-10-82543785; zhaobz@nanoctr.cn or baozhongus@gmail.com (B. Zhao).

[1]J.J. Yin and J. Liu contributed equally to this paper.

Conflict of interest statement

The authors declare that there are no conflicts of interest.

Keywords

TiO_2 nanoparticles; Phototoxicity; Reactive oxygen species (ROS); Lipid peroxidation; Human HaCaT keratinocytes; ESR; Oximetry; Immuno-spin trapping

Introduction

Nanomaterials have been recently developed that show great potential for use in the biomedical, optical, and electronic fields. They are currently manufactured on a large scale to be used in thousands of consumer goods and industrial products. However, nanomaterials are potentially toxic due to their unique properties including extremely high surface-to-volume ratios, which can make them very reactive or catalytic. Furthermore, the tiny size of nanomaterials makes it possible for them to pass through cell membranes and other biological barriers. Therefore, investigation of cellular toxicity and phototoxicity of nanomaterials is critically needed.

Nano-sized titanium dioxide (TiO_2) is among the top five nanomaterials widely used in paints, plastics, cosmetics, personal care products, and as food additives and drug delivery agents (Kangwansupamonkon *et al.*, 2009; Ray *et al.*, 2009). The usefulness of TiO_2 nanoparticles (nano-TiO_2) is primarily linked to two of its functions: absorbing and deflecting ultraviolet (UV) radiation and semiconductor photocatalysis (Fujishima *et al.*, 2000). Under UVA irradiation, electrons in the TiO_2 valence band absorb the photon energy and jump to the conduction band, leaving valence band holes that extract electrons from water or hydroxyl ions and generate hydroxyl radicals ($^{\bullet}OH$). Formation of other reactive oxygen species (ROS), including superoxide ($O_2^{\bullet -}$) and singlet oxygen ($^1O_2$), by different mechanisms has also been reported (Hirakawa and Hirano, 2006; Daimon and Nosaka, 2007). The photocatalytic properties make TiO_2 nanoparticles successful candidates for degrading organic pollutants (Mura *et al.*, 1999) or killing microorganisms (Kangwansupamonkon *et al.*, 2009; Foster *et al.*, 2011). On the other hand, potential risks associated with exposure to nano-TiO_2 raise many concerns due to generation of ROS during UV irradiation; ROS are genotoxic or cytotoxic to organisms (Vevers and Jha, 2008; Ghosh *et al.*, 2010; Sycheva *et al.*, 2011).

Previous studies have suggested that nano-TiO_2 that has not been irradiated with UV has limited cytotoxicity (Rehn *et al.*, 2003). However, further reports have shown that TiO_2 particles without illumination affected cell-matrix adhesion, which is not associated with ROS damage to cells (Fujita *et al.*, 2009). Under UV irradiation, TiO_2 nanoparticles exhibit toxic effects to both normal tissue and cancer cells, such as human dermal and lung cells (Liao *et al.*, 2009), human keratinocyte cells (Shukla *et al.*, 2011; Simon *et al.*, 2011), rat lung alveolar macrophages (Afaq *et al.*, 1998), intestinal cells (Koeneman *et al.*, 2010) and HeLa cells (Cai *et al.*, 1992). The human skin and eye are of particular concern as target sites for phototoxic damage because these tissues are constantly exposed to direct daily ambient radiation. It was reported that although micron-sized TiO_2 cannot penetrate through the intact epidermal barrier (Kiss *et al.*, 2008), topical application of TiO_2 nanoparticles may induce dermal toxicity (Wu *et al.*, 2009). The photoreactivity of TiO_2 nanoparticles is largely dependent on their particle size, shape and crystal structure (Sharma, 2009; Liu *et al.*, 2010). It was demonstrated that smaller nano-TiO_2 particles tend to have higher phototoxicity, and anatase and amorphous forms of nano-TiO_2 show higher cytotoxicity than its rutile form (Xue *et al.*, 2010; Sanders *et al.*, 2011).

In the present studies, we have evaluated the phototoxicity of nano-TiO_2 with four different sizes (<25 nm, 31 nm, <100 nm, and 325 nm) and two crystal forms (anatase and rutile)

towards human skin keratinocytes under UVA irradiation. We observe that their differences in phototoxicity are highly correlated with the production of ROS. By employing polyunsaturated lipids in plasma membrane and human serum albumin (HSA) as model targets, our unique electron spin resonance (ESR) oximetry and immuno-spin trapping techniques indicate that UVA photoirradiation of nano-TiO_2 in biological systems can lead to significant cell damage.

Materials and methods

Chemicals

Nano-TiO_2 (A25, <25 nm anatase, catalog # 637254; A325, 325 mesh anatase, catalog # 248576; R100, <100 nm rutile, catalog # 637262), HSA, xanthine, superoxide dismutase (SOD), diethylenetriaminepentaacetic acid (DTPA), 2,2,6,6-tetramethyl-4-piperidone (TEMP) and dimethyl sulfoxide (DMSO, cell-culture grade) were all purchased from Sigma Chemical Co. (St. Louis, MO). Titanium dioxide (P25, 31 nm anatase/rutile, catalog # Aeroxide® TiO_2 P25) was from Degussa (Alpharetta, GA). Fetal bovine serum (FBS) was from Biofluids (Rockville, MD, USA). Dulbecco's modified Eagle's medium (DMEM), phosphate buffered saline (PBS, pH 7.4), trypsin-EDTA, penicillin, and streptomycin were purchased from Invitrogen Inc. (Grand Island, NY). The MTS assay kit (CellTiter 96® Aqueous) was purchased from Promega Co. (Madison, WI). ^{15}N-labeled 4-oxo-2,2,6,6-tetramethylpiperidine-d16-1-oxyl (^{15}N-PDT) was purchased from Cambridge Isotope Labs (Andover, MA). Xanthine oxidase (XOD) was from Roche Applied Science (Indianapolis, IN). The spin-trap 5-tert-butoxycarbonyl 5-methyl-1-pyrroline *N*-oxide (BMPO) was purchased from Applied Bioanalytical Labs (Sarasota, FL). Egg phosphatidylcholine was obtained from Avanti Polar Lipids, Inc. (Alabaster, AL). 5,5-dimethy-1-pyrroline *N*-oxide (DMPO) was purchased from Dojindo laboratories (Japan).

Preparation of TiO_2 suspensions

The nano-TiO_2 suspensions were prepared by first dispersing the nanoparticles in ultrapure water using a sonicator for 30 min to produce a 10 mg/ml stock nano-TiO_2 suspension and then diluting according to the requirements of the experiments.

Characterization of nano-TiO_2

X-ray diffraction (XRD) patterns were recorded on a Philips XPert PRO MPD X-ray diffractometer (Philips, Eindhoven, The Netherlands) operated at 35 kV and 45 mA with Cu-Kα radiation. Scanning Electron Microscope (SEM) images were taken on a Hitachi S4800 field scanning electron microscope (FESEM, Japan) operating at 10 kV. Samples were suspended in ethanol solution by sonication first. Approximately 10 μl of suspensions were spin-coated on a silicon wafer at 3000 rpm for 60 seconds. Dynamic light scattering (DLS) measurements of particle size were carried out using a light scattering Zetasizer Nano-S90 light scattering instrument (Malvern Instruments, Enigma Business Park, UK).

Cell culture and phototoxicity measurement

Human HaCaT keratinocytes, a transformed epidermal human cell line (Boukamp *et al.*, 1988), were grown to ~95% confluence in 96-well plates at 37ºC in DMEM containing 10% FBS under 95% air/5% CO_2. For phototoxicity tests, cells were exposed in the dark for 4 h at 37 ºC to different TiO_2s (50 and100 μg/ml) in DMEM (FBS free). Control cells were treated with DMEM alone. After incubation the medium was removed and replaced by sterile PBS containing 10 mM glucose. Cells were then irradiated with UVA from four fluorescent PUVA lamps (Houvalite F20T12BL-HO; National Biological Co. Twinsburg, OH). The maximum emission of the UVA light lamps was determined to be between 320–

390 nm. The light intensities at wavelengths below 315 nm (UVB light) and above 400 nm (visible light) are approximately two orders of magnitude lower than the maximum in the 320–390 nm spectral region (Zhao *et al.*, 2010). The UVA exposure doses were 0, 2.5, 5.0, and 10 J/cm^2 respectively, as measured with an YSI-Kettering Model 65A Radiometer (Yellow Springs Instrument Co., Yellow Springs, OH). After exposure the PBS/glucose solution was removed and replaced with DMEM containing 2% FBS and the cells were kept in the incubator overnight. Aliquots (10 μl) were removed and LDH release into the medium was assayed using the Cytotox 96 kit (Promega Corp., Madison, WI) according to the manufacturer's directions. The remaining medium was removed and the cells were washed with PBS and replaced with 100 μl/well of PBS/glucose containing the MTS reagent (CellTiter 96 Aqueous Proliferation Assay; Promega Cop.). After incubation for 2 h at 37 ºC, the absorbance at 492 nm was recorded using a microplate reader (Spectrafluor Plus, Tecan US, RTP, NC).

ESR spectroscopy

Conventional ESR spectra were obtained with a Bruker EMX ESR Spectrometer (Billerica, MA). All spin trapping ESR measurements were carried out using the following settings for detection of the spin adduct between BMPO and $O_2^{\bullet-}$ (BMPO-OH): 10 mW microwave power, 100 G scan range and 1 G field modulation. All measurements were performed in replicates at ambient temperature. A light system consisting of a Xenon lamp coupled with a Schoeffel monochromator was used to generate UV light at 340 nm wavelength. All the samples for ESR measurements were freshly prepared in 100 mM phosphate buffer at pH 7.4. The buffer was treated with Chelex-100 resin for 24 h to remove traces of transition metal ions.

Spin label oximetry

ESR oximetry measurement is based on the bimolecular collision of molecular oxygen with a spin label which is a stable free radical. Collision of the spin label with O_2 produces a spin exchange, resulting in shorter relaxation times and ESR signals with broader linewidths and decreasing peak height. Thus, oxygen consumption by such mechanisms as lipid peroxidation results in decreased line widths and increased peak height for the spin probe. The oximetry method determines the oxygen concentration by measuring the hyperfine structural changes at the low field line of the ESR spectrum using ^{15}N-PDT as the spin label (Halpern *et al.*, 1994; Swartz and Clarkson, 1998; Xia *et al.*, 2007; Yin *et al.*, 2008; Yin *et al.*, 2009). During lipid peroxidation, the levels of dissolved O_2 vary, with a time dependent decrease in linewidth and an increase in the peak intensity of the ESR signal indicating continuous O_2 consumption. The value of oxygen concentration was obtained from a calibrated curve of the ESR linewidth versus the oxygen concentration.

Liposomes were prepared as previously described (Kusumi *et al.*, 1986). Briefly, a suspension of 30 mg/ml egg PC liposomes and 0.1mM ^{15}N-PDT with or without TiO_2 was added to a quartz capillary tube. The lipid peroxidation was initiated by UV (340 nm) irradiation. The ESR spectra were then recorded at 4 min intervals for 16 min. Signals were obtained with a 0.05 G scanning width, 0.5 mW incident microwave power and with 100 kHz field modulation. All ESR spectra were recorded at the low field line of ^{15}N-PDT and at ambient temperature.

ELISA and Western Blot

HSA protein samples were typically prepared by treating 600 μM HSA with 0.1 mg/ml TiO_2, and 50 mM DMPO in 100 mM phosphate buffer (Chelex-treated with 25 μM DTPA) at pH 7.4 in a 6-well plate in the absence or presence of UVA irradiation (10 J/cm^2). After treatment, samples were frozen at -80 ºC for further experiments.

The ELISA assay to measure DMPO nitrone adducts was performed essentially as described by Ehrenshaft and Mason (Ehrenshaft and Mason, 2006) with minor modifications. Two microgram aliquots of protein diluted in bicarbonate buffer, pH 9.4, were allowed to adsorb to the wells of a 96-well microtiter plate (Grenier Labortechnik) for 1.5 h. After washing once with wash buffer (1×PBS with 0.1% tween), the microtiter plate was incubated for 1 h in a 1:5000 dilution of rabbit polyclonal anti-DMPO antiserum, washed 4 times with wash buffer, incubated for 1 h more in a 1:5000 dilution of an alkaline phosphatase anti-rabbit secondary antibody, again washed 4 times with wash buffer, and finally washed once with 1×TBS, pH 9.6. After addition of CDP-Star (25 μM) (Roche Laboratories), the chemiluminescent product was detected using a microplate reader (Spectrafluor Plus, Tecan US, RTP, NC).

For Western Blot analysis, 10 μg of HSA protein from each reaction were electrophoresed under reducing conditions through a 4–12% BisTris NuPAGE acrylamide gel (Invitrogen) followed by electroblotting to a nitrocellulose membrane. Western Blot analysis was then performed as described (Ehrenshaft and Mason, 2006) except that DMPO-containing proteins were visualized using the Odyssey infrared imaging system (Licor).

Results

Characterization of nano-TiO_2

The XRD results shown in Fig. 1A reveal the crystal structure of nano-TiO_2 samples, which are consistent with the crystallinity provided by the vendors. The crystalline composition of P25 was evaluated to be around 86% anatase and 14% rutile by the ratios of the integral areas of the three main diffraction peaks of the two phases (Zhao *et al.*, 2008). SEM was used to visualize the particle size and shape of nano-TiO_2. The SEM images of four nano-TiO_2 samples are shown in Fig. 1B. The sizes are roughly consistent with the sizes claimed by the vendors. From the SEM images we also find that aggregates or big clusters are formed for all samples, especially for the smallest A25 sample. DLS measurements show the size and distribution of TiO_2 aggregates in the aqueous medium, which are largely dependent on the concentration, dispersant, and primary particle size (Sanders *et al.*, 2011). As shown in Fig. 1C, aggregates of the smallest A25 sample were between 150–500 nm and the other three were between roughly 250–700 nm at the lower concentration (50 μg/mL) tested in the phototoxicity experiments.

Nano-TiO_2-induced phototoxicity in human HaCaT keratinocytes

The phototoxicity of the four different sizes of nano-TiO_2 towards HaCaT keratinocytes was determined using two different assays. The MTS assay measures the activity of (mainly mitochondrial) dehydrogenases, while cell membrane damage is measured by the release of cytosolic LDH. As measured by the MTS assay, no decrease in viability was observed when HaCaT cells were exposed to TiO_2 samples or to UVA alone (Fig. 2A and 2B). However, in the presence of UVA radiation, two anatase TiO_2 samples (A325 and A25) and P25 TiO_2 caused UVA dose- and concentration-dependent damage to HaCaT cells. The rutile TiO_2 sample (R100) showed much less phototoxicity towards HaCaT cells even at a high concentration of 100 μg/ml and 10 J/cm^2 UVA exposure (Fig. 2B). The extent of photocytotoxicity to cells irradiated at 7.5 or 10 J/cm^2 was in the following order: P25>A25>A325>R100. A similar result was seen with the LDH release assay (Fig. 3A and 3B).

ESR measurement of ROS generation

ESR spin trap spectroscopy was employed to determine whether or not nano-TiO_2 under UVA light irradiation has the capability to generate ROS chemically. Generation of

hydroxyl radicals was detected by the ESR spin trapping technique using BMPO. BMPO is a newly developed spin trap offering more advantages over the existing spin traps, such as greater stability and sensitivity (Zhao *et al.*, 2001). The BMPO/$^{\bullet}$OH adduct has an ESR signal pattern similar to that of DMPO/$^{\bullet}$OH, which exhibits a characteristic set of four lines (1:2:2:1) in its ESR spectrum. In the absence of UVA irradiation, the ESR signal of the hydroxyl radical spin adduct was not detectable from the mixture of BMPO and nano-TiO_2 (data not shown). No such ESR profile was generated when BMPO was irradiated under UVA light (340 nm) in the absence of nano-TiO_2 (Fig. 4A) or in the presence of the rutile R100 TiO_2 sample (Fig. 4B). However, UVA irradiation of BMPO in the presence of A325 nano-TiO_2, A25 nano-TiO_2, or P25 nano-TiO_2 all produced the characteristic ESR profile (Fig. 4C, 4D, and 4E). As shown in Fig. 4, UVA irradiation of P25 nano-TiO_2 resulted in the strongest signal of BMPO/$^{\bullet}$OH signal (Fig. 4E), followed by two anatase TiO_2 samples, A325 nano-TiO_2 and A25 nano-TiO_2 (Fig. 4C and 4D). This signal was largely inhibited by the addition of 20% DMSO (Fig. 4F), further confirming the generation of OH radicals during the UVA irradiation.

We tested the generation of singlet oxygen by the ESR trapping technique using TEMP. It has been previously reported that 4-oxo-2,2,6,6-tetramethylpiperidine-N-oxyl (TEMPONE), a nitroxide radical detectable by EPR spectra, is generated from TEMP and singlet oxygen (Eq. 1) (Lion *et al.*, 1976).

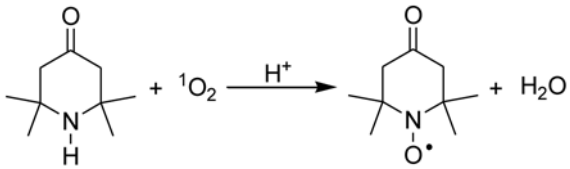

(1)

Irradiation of different nano-TiO_2 samples (0.1 mg/ml) containing 20 mM TEMP resulted in ESR spectra of three lines with equal intensities (a_N = 16.0 G), typical of nitroxide radicals (Fig. 5, inset). The hyperfine splitting constant and g factor of the photosensitized oxidation product of TEMP were identical to those of commercial TEMPONE. Fig. 5 shows the ESR intensity of the TEMPONE signal as a function of time during irradiation of different nano-TiO_2 samples. The P25 nano-TiO_2 solution (Fig. 5, curve A) showed the rate that increased the fastest, followed by the A25 nano-TiO_2 sample (Fig. 5, curve B). The rates of production of singlet oxygen were much slower for A325 nano-TiO_2 and R100 nano-TiO_2 (Fig. 5, curves C and D). A control solution with TEMP only (data not shown) indicated no ESR signal increase. For P25 nano-TiO_2, addition of a singlet oxygen quencher, NaN_3, caused a substantial decrease in the rate of increase of the EPR signal (Fig. 5, curve E).

It has been reported that $O_2^{\bullet-}$ can be oxidized to $^1O_2$ during TiO_2 photocatalytic reactions (Lipovsky *et al.*, 2012). Superoxide ($O_2^{\bullet-}$) undergoes dismutation to produce H_2O_2, from which the $^{\bullet}$OH radical can also be formed through the Fenton reaction. To further elucidate the mechanisms of $^{\bullet}$OH and $^1O_2$ generation, we studied the effect of SOD on the production of $^{\bullet}$OH and $^1O_2$ by P25 nano-TiO_2 during UVA irradiation. As a control study, addition of 1.25 U/ml SOD significantly inhibited the production of $O_2^{\bullet-}$ generated in a Xanthine system (Fig. 6A and 6B). However, no obvious effect was observed on $^{\bullet}$OH generation by P25 nano-TiO_2 under UVA irradiation even at a high concentration of SOD (6 U/ml, Fig. 6C and 6D), indicating that nano-TiO_2-generated $^{\bullet}$OH radicals were not evolved from $O_2^{\bullet}$, at least for the most part. In contrast, the $^1O_2$ generation was markedly reduced in the presence of 1.25 U/ml SOD (Fig. 6E and 6F), confirming that $O_2^{\bullet-}$ may be a main pathway

in UVA-induced $^1O_2$ generation by nano-TiO_2 (Lipovsky *et al.*, 2012). It is noteworthy that although $O_2^{\bullet -}$ was formed from UVA irradiation of nano-TiO_2 and was attributed to the formation of $^1O_2$, no obvious $O_2^{\bullet -}$ production was detected in our ESR study using BMPO as a trapping agent (Fig. 4), which is actually consistent with a previous report (Konaka *et al.*, 2001). Its short lifetime under our experimental conditions warrants further investigation.

ESR oximetry measurement of lipid peroxidation

It is well known that ROS can produce a time-dependent peroxidation of the polyunsaturated lipids in plasma membrane. In this study, lipid peroxidation produced by UVA irradiation of different nano-TiO_2 was assessed using ESR oximetry recorded at 4-min intervals for 16 min. The consumption of oxygen accompanying lipid peroxidation was measured as a time-dependent narrowing of the ESR signal for the spin probe ^{15}N-PDT. As shown in Fig. 7, narrowing of the ESR signal was necessarily accompanied by an increase in the peak height of the ESR signal within the scan range. The results of lipid peroxidation produced by different nano-TiO_2 samples (R100, A325, A25, and P25) after UVA irradiation are shown in Fig. 7B–7E, respectively. The final ESR signal intensities of R100 nano-TiO_2 (Fig. 7B), A325 nano-TiO_2 (Fig. 7C), A25 nano-TiO_2 (Fig. 7D), and P25 nano-TiO_2 (Fig. 7E) were approximately 7.5, 11.7, 16.2, and 26.3% higher than in the control (Fig. 7A). The progressive increases in peak-to-peak signal intensity (and accompanying progressive narrowing of line width) in each panel were due to time-dependent oxygen consumption resulting from lipid peroxidation. Fig. 6F presents the data as a decrease in oxygen concentration, reflecting the variations in the slope (oxygen concentration versus time) with different nano-TiO_2, which decreases in the order of P25 > A25 > A325 > R100.

Immuno-spin trapping measurement of protein radicals

To further characterize the ability of ROS to oxidize target proteins, the most abundant plasma protein (human serum albumin, HSA) was incubated with DMPO and different nano-TiO_2 samples with and without UVA irradiation. The reaction products were analyzed by ELISA and Western blotting using an anti-DMPO polyclonal antibody. Immunochemical detection of HSA-DMPO nitrone adducts was performed according to our previous studies (Ranguelova *et al.*, 2010). As measured by both ELISA and Western blotting, HSA with DMPO exposed to different nano-TiO_2 samples or UVA alone produced nitrone adducts at background levels (Fig. 8A–8E). While in the presence of UVA irradiation, P25 nano-TiO_2 resulted in a significant increase in HSA-DMPO-derived nitrone adducts (Fig. 8I). The other three nano-TiO_2 samples caused modest increases in adduct formation (Fig. 8F–8H). The order of the extent of nitrone adducts is the same as for photocytotoxicity, hydroxyl radical, singlet oxygen, and lipid peroxidation measurements.

Discussion

TiO_2 is regarded as an inert and non-toxic substance by many regulatory bodies; e.g., the FDA approved TiO_2 as a food color additive in 1996, and the Material Safety Data Sheets (MSDS) indicate that there are no exposure hazards to the health of occupational workers and public health. However, there have been several studies that have shown that TiO_2 is a potential carcinogen and photocatalyst in biological tissues (Burnett and Wang, 2011). The cytotoxicity and/or phototoxicity of nano-TiO_2 is still debated. Also, there is uncertainty about whether the properties of nano-TiO_2 differ with its particular form and size. Human skin and ocular tissues are most affected by ambient radiation. In vitro studies have shown that when irradiated, the smallest form of TiO_2, anatase (<25 nm), is phototoxic to human retinal cells (Sanders *et al.*, 2011). UV-induced production of ROS and the resultant oxidative stress exposure plays an important role in photocarcinogenesis caused by UV

irradiation. ROS are believed to be involved in many inflammatory skin disorders, skin cancer formation, and skin aging (He *et al.*, 2005). Thus we report here a study of the photocytotoxicity and phototoxicity of nano-TiO_2 towards human HaCaT keratinocytes.

Our results show that all nano-TiO_2 tested in this paper caused UVA and nano-TiO_2 dose-dependent phototoxicity in HaCaT cells. As expected, smaller particles resulted in higher phototoxicity than larger particles. Rutile nano-TiO_2 showed less phototoxicity than anatase nano-TiO_2. Moreover, small mixed anatase/rutile nano-TiO_2 (P25) showed the highest phototoxicity, which is consistent with previous reported results (Hurum *et al.*, 2003). The cellular toxicity of nano-TiO_2 mainly depends on its ROS generation under UVA irradiation. Using ESR and spin trapping technique, a “gold standard” and state-of-the-art tool for detecting and quantifying ROS, we confirmed the generation of hydroxyl radicals and singlet oxygen. ROS generation by these four nano-TiO_2 particles is consistent with the phototoxicity studies, further confirming our hypothesis that ROS production was probably involved in the phototoxic mechanism.

In addition to measurement of ROS generation with ESR, we explored two other assays to further characterize the phototoxicity of nano-TiO_2. ROS are known to produce a time-dependent peroxidation of the polyunsaturated lipids in plasma membrane (Yin *et al.*, 2008; Yin *et al.*, 2009) as well as peroxidation of lipids and proteins inside the cells (Girotti, 1998). To mimic oxidation reactions with substrates in biological systems, we used polyunsaturated lipids in plasma membranes and human serum albumin as model targets for ROS. Using innovative ESR oximetry and immune-spin trapping techniques, we easily detected ROS-induced peroxidation, which was found to be in agreement with the ESR-detected ROS production. These results indicate that both methods are useful for qualitative screening of the phototoxicity of nano-TiO_2.

Based on the results reported in this study, we propose the mechanism shown in Fig. 9. UVA irradiation results in electron-hole pairs in nano-TiO_2. The photoexcited nano-TiO_2 serves as the initiating species to transfer energy to molecular oxygen and generate singlet oxygen ($^1O_2$) or to extract electrons from water or hydroxyl ions to generate hydroxyl radicals ($^{\bullet}OH$). Our experimental results also indicate that part of the $^1O_2$ formation proceeds via a superoxide-dependent mechanism, whereas the OH formation is not via superoxide (Fig. 6). It is well established that in the presence of a lipid or protein, the generated ROS can initiate lipid and/or protein peroxidation. Both ROS and lipid peroxidation are associated with aging-related diseases, including cancer (Aust *et al.*, 1993; Xia *et al.*, 2007).

In conclusion, the studies presented here give an overall *in vitro* assessment of the phototoxicity by various nano-TiO_2 particles towards HaCaT cells under UVA irradiation. This phototoxic damage was apparently mediated by production of ROS by photo-activated nano-TiO_2. According to our results ROS are generated by UVA irradiation of nano-TiO_2 with anatase and/or mixed anatase/rutile forms. Moreover, the phototoxicity of nano-TiO_2 was less with larger particle size and surface areas, indicating that coarse particles of nano-TiO_2 may consistently produce less ROS.

Acknowledgments

This article is not an official US Food and Drug Administration (FDA) guidance or policy statement. No official support or endorsement by the US FDA is intended or should be inferred. This work was supported by a regulatory science grant under the FY11 FDA Nanotechnology CORES Program (JJ Yin) and the Intramural Research Program of the NIH, National Institute of Environmental Health Sciences. The authors are indebted to Dr. Jianxun Xu for his help in SEM image analysis, Dr. Zhanjun Gu, Yeteng Zhong for their help in XRD analysis, and Dr. Ann Motten, NIEHS, for critical reading of the manuscript.

Abbreviations

^{15}N-PDT	4-Oxo-2,2,6,6-tetramethylpiperidine-d16-1-oxyl
BMPO	5-tert-butoxycarbonyl 5-methyl-1-pyrroline *N*-oxide
DLS	dynamic light scattering
DMEM	Dulbecco's modified Eagle's medium
DMPO	5,5-dimethy-1-pyrroline *N*-oxide
DMSO	dimethyl sulfoxide
ESR	electron spin resonance
FBS	fetal bovine serum
DTPA	diethylenetriaminepentaacetic acid
HSA	human serum albumin
LDH	lactate dehydrogenase
MTS	3-(4,5-dimethylthiazol-2-yl)-5-(3-carboxymethoxyphenyl)-2-(4-sulfophenyl)-2H-tetrazolium
PBS	phosphate buffered saline
ROS	reactive oxygen species
SEM	scanning electron microscopy
SOD	superoxide dismutase
TEMP	2,2,6,6-tetramethyl-4-piperidone
UVA	ultraviolet A (315-400 nm)
XOD	xanthine oxidase
XRD	X-ray diffraction

References

Afaq F, Abidi P, Matin R, Rahman Q. Cytotoxicity, pro-oxidant effects and antioxidant depletion in rat lung alveolar macrophages exposed to ultrafine titanium dioxide. J Appl Toxicol. 1998; 18:307–312. [PubMed: 9804429]

Aust SD, Chignell CF, Bray TM, Kalyanaraman B, Mason RP. Free radicals in toxicology. Toxicol Appl Pharmacol. 1993; 120:168–178. [PubMed: 8511786]

Boukamp P, Petrussevska RT, Breitkreutz D, Hornung J, Markham A, Fusenig NE. Normal keratinization in a spontaneously immortalized aneuploid human keratinocyte cell line. J Cell Biol. 1988; 106:761–771. [PubMed: 2450098]

Burnett ME, Wang SQ. Current sunscreen controversies: a critical review. Photodermatol Photo. 2011; 27:58–67.

Cai R, Kubota Y, Shuin T, Sakai H, Hashimoto K, Fujishima A. Induction of cytotoxicity by photoexcited TiO2 particles. Cancer Res. 1992; 52:2346–2348. [PubMed: 1559237]

Daimon T, Nosaka Y. Formation and behavior of singlet molecular oxygen in TiO2 photocatalysis studied by detection of near-infrared phosphorescence. J Phys Chem C. 2007; 111:4420–4424.

Ehrenshaft M, Mason RP. Protein radical formation on thyroid peroxidase during turnover as detected by immuno-spin trapping. Free Radical Bio Med. 2006; 41:422–430. [PubMed: 16843823]

Foster HA, Ditta IB, Varghese S, Steele A. Photocatalytic disinfection using titanium dioxide: spectrum and mechanism of antimicrobial activity. Appl Microbiol Biot. 2011; 90:1847–1868.

Fujishima A, Rao TN, Tryk DA. Titanium dioxide photocatalysis. J Photoch Photobio C. 2000; 1:1–21.

Fujita K, Horie M, Kato H, Endoh S, Suzuki M, Nakamura A, Miyauchi A, Yamamoto K, Kinugasa S, Nishio K, Yoshida Y, Iwahashi H, Nakanishi J. Effects of ultrafine TiO(2) particles on gene expression profile in human keratinocytes without illumination: Involvement of extracellular matrix and cell adhesion. Toxicol Lett. 2009; 191:109–117. [PubMed: 19695317]

Ghosh M, Bandyopadhyay M, Mukherjee A. Genotoxicity of titanium dioxide (TiO2) nanoparticles at two trophic levels: plant and human lymphocytes. Chemosphere. 2010; 81 :1253–1262. [PubMed: 20884039]

Girotti AW. Lipid hydroperoxide generation, turnover, and effector action in biological systems. J Lipid Res. 1998; 39:1529–1542. [PubMed: 9717713]

Halpern HJ, Yu C, Peric M, Barth E, Grdina DJ, Teicher BA. Oxymetry deep in tissues with low-frequency electron paramagnetic resonance. P Nat Acad Sci USA. 1994; 91:13047–13051.

He YY, Huang JL, Block ML, Hong JS, Chignell CF. Role of phagocyte oxidase in UVA-induced oxidative stress and apoptosis in keratinocytes. J Invest Dermatol. 2005; 125:560–566. [PubMed: 16117799]

Hirakawa K, Hirano T. Singlet oxygen generation photocatalyzed by TiO2 particles and its contribution to biomolecule damage. Chem Lett. 2006; 35:832–833.

Hurum DC, Agrios AG, Gray KA, Rajh T, Thurnauer MC. Explaining the enhanced photocatalytic activity of Degussa P25 mixed-phase TiO2 using EPR. J Phys Chem B. 2003; 107:4545–4549.

Kangwansupamonkon W, Lauruengtana V, Surassmo S, Ruktanonchai U. Antibacterial effect of apatite-coated titanium dioxide for textiles applications. Nanomedicine : NBM. 2009; 5:240–249.

Kiss B, Biro T, Czifra G, Toth BI, Kertesz Z, Szikszai Z, Kiss AZ, Juhasz I, Zouboulis CC, Hunyadi J. Investigation of micronized titanium dioxide penetration in human skin xenografts and its effect on cellular functions of human skin-derived cells. Exp Dermatol. 2008; 17:659–667. [PubMed: 18312389]

Koeneman BA, Zhang Y, Westerhoff P, Chen YS, Crittenden JC, Capco DG. Toxicity and cellular responses of intestinal cells exposed to titanium dioxide. Cell Biol Toxicol. 2010; 26:225–238. [PubMed: 19618281]

Konaka R, Kasahara E, Dunlap WC, Yamamoto Y, Chien KC, Inoue M. Ultraviolet irradiation of titanium dioxide in aqueous dispersion generates singlet oxygen. Redox Rep. 2001; 6:319–325. [PubMed: 11778850]

Kusumi A, Subczynski WK, Pasenkiewicz-Gierula M, Hyde JS, Merkle H. Spin-label studies on phosphatidylcholine-cholesterol membranes: effects of alkyl chain length and unsaturation in the fluid phase. Biochim Biophys Acta. 1986; 854:307–317. [PubMed: 3002470]

Liao CM, Chiang YH, Chio CP. Assessing the airborne titanium dioxide nanoparticle-related exposure hazard at workplace. J Hazard Mater. 2009; 162:57–65. [PubMed: 18554790]

Lion Y, Delmelle M, van de Vorst A. New method of detecting singlet oxygen production. Nature. 1976; 263:442–443. [PubMed: 972689]

Lipovsky A, Levitski L, Tzitrinovich Z, Gedanken A, Lubart R. The different behavior of rutile and anatase nanoparticles in forming oxy radicals upon illumination with visible light: an EPR study. Photochem Photobiol. 2012; 88:14–20. [PubMed: 21988075]

Liu R, Yin LH, Pu YP, Li YH, Zhang XQ, Liang GY, Li XB, Zhang JA, Li YF, Zhang XY. The Immune Toxicity of Titanium Dioxide on Primary Pulmonary Alveolar Macrophages Relies on their Surface Area and Crystal Structure. J Nanosci Nanotechno. 2010; 10:8491–8499.

Mura GM, Ganadu ML, Lubinu G, Maida V. Photodegradation of organic waste coupling hydrogenase and titanium dioxide. Ann NY Acad Sci. 1999; 879:267–275. [PubMed: 10415838]

Ranguelova K, Bonini MG, Mason RP. (Bi)sulfite oxidation by copper, zinc-superoxide dismutase: Sulfite-derived, radical-initiated protein radical formation. Environ Health Persp. 2010; 118:970–975.

Ray PC, Yu H, Fu PP. Toxicity and environmental risks of nanomaterials: challenges and future needs. J Environ Sci Heal C Environ Carcinog Ecotoxicol Rev. 2009; 27 :1–35.

Rehn B, Seiler F, Rehn S, Bruch J, Maier M. Investigations on the inflammatory and genotoxic lung effects of two types of titanium dioxide: untreated and surface treated. Toxicol Appl Pharm. 2003; 189:84–95.

Sanders K, Degn LL, Mundy WR, Zucker RM, Dreher K, Zhao B, Roberts JE, Boyes WK. In Vitro Phototoxicity and Hazard Identification of Nano-scale Titanium Dioxide. Toxicol Appl Pharmacol. 2011; 258:226–236. [PubMed: 22115978]

Sharma VK. Aggregation and toxicity of titanium dioxide nanoparticles in aquatic environment-A Review. J Environ Sci Heal A. 2009; 44:1485–1495.

Shukla RK, Kumar A, Pandey AK, Singh SS, Dhawan A. Titanium Dioxide Nanoparticles Induce Oxidative Stress-Mediated Apoptosis in Human Keratinocyte Cells. J Biomed Nanotechnol. 2011; 7:100–101. [PubMed: 21485823]

Simon M, Barberet P, Delville MH, Moretto P, Seznec H. Titanium dioxide nanoparticles induced intracellular calcium homeostasis modification in primary human keratinocytes. Towards an in vitro explanation of titanium dioxide nanoparticles toxicity. Nanotoxicology. 2011; 5:125–139. [PubMed: 21425910]

Swartz HM, Clarkson RB. The measurement of oxygen in vivo using EPR techniques. Phys Med Biol. 1998; 43:1957–1975. [PubMed: 9703059]

Sycheva LP, Zhurkov VS, Iurchenko VV, Daugel-Dauge NO, Kovalenko MA, Krivtsova EK, Durnev AD. Investigation of genotoxic and cytotoxic effects of micro- and nanosized titanium dioxide in six organs of mice in vivo. Mutat Res. 2011; 726:8–14. [PubMed: 21871579]

Vevers WF, Jha AN. Genotoxic and cytotoxic potential of titanium dioxide (TiO2) nanoparticles on fish cells in vitro. Ecotoxicology. 2008; 17:410–420. [PubMed: 18491228]

Wu J, Liu W, Xue C, Zhou S, Lan F, Bi L, Xu H, Yang X, Zeng FD. Toxicity and penetration of TiO2 nanoparticles in hairless mice and porcine skin after subchronic dermal exposure. Toxicol Lett. 2009; 191:1–8. [PubMed: 19501137]

Xia Q, Yin JJ, Fu PP, Boudreau MD. Photo-irradiation of Aloe vera by UVA--formation of free radicals, singlet oxygen, superoxide, and induction of lipid peroxidation. Toxicol Lett. 2007; 168:165–175. [PubMed: 17197137]

Xue C, Wu J, Lan F, Liu W, Yang X, Zeng F, Xu H. Nano titanium dioxide induces the generation of ROS and potential damage in HaCaT cells under UVA irradiation. J Nanosci Nanotechnol. 2010; 10:8500–8507. [PubMed: 21121359]

Yin JJ, Lao F, Fu PP, Wamer WG, Zhao Y, Wang PC, Qiu Y, Sun B, Xing G, Dong J, Liang XJ, Chen C. The scavenging of reactive oxygen species and the potential for cell protection by functionalized fullerene materials. Biomaterials. 2009; 30:611–621. [PubMed: 18986699]

Yin JJ, Lao F, Meng J, Fu PP, Zhao Y, Xing G, Gao X, Sun B, Wang PC, Chen C, Liang XJ. Inhibition of tumor growth by endohedral metallofullerenol nanoparticles optimized as reactive oxygen species scavenger. Mol Pharmacol. 2008; 74:1132–1140. [PubMed: 18635669]

Zhao B, Chignell CF, Rammal M, Smith F, Hamilton MG, Andley UP, Roberts JE. Detection and prevention of ocular phototoxicity of ciprofloxacin and other fluoroquinolone antibiotics. Photochem Photobiol. 2010; 86:798–805. [PubMed: 20528972]

Zhao H, Joseph J, Zhang H, Karoui H, Kalyanaraman B. Synthesis and biochemical applications of a solid cyclic nitrone spin trap: a relatively superior trap for detecting superoxide anions and glutathiyl radicals. Free Radical Bio Med. 2001; 31:599–606. [PubMed: 11522444]

Zhao L, Han M, Lian H. Photocatalytic activity of TiO2 films with mixed anatase and rutile structures prepared by pulsed laser deposition. Thin Solid Films. 2008; 516:3394–3398.

Highlights

- We evaluate the phototoxicity of nano-TiO_2 with different sizes and crystal forms.
- The smaller the particle size of nano-TiO_2 the higher the cell damage.
- The rutile form of nano-TiO_2 showed less phototoxicity than anatase nano-TiO_2.
- ESR oximetry and immuno-spin trapping techniques confirm UVA-induced cell damage.
- Phototoxicity is mediated by ROS generated during UVA irradiation of nano-TiO_2.

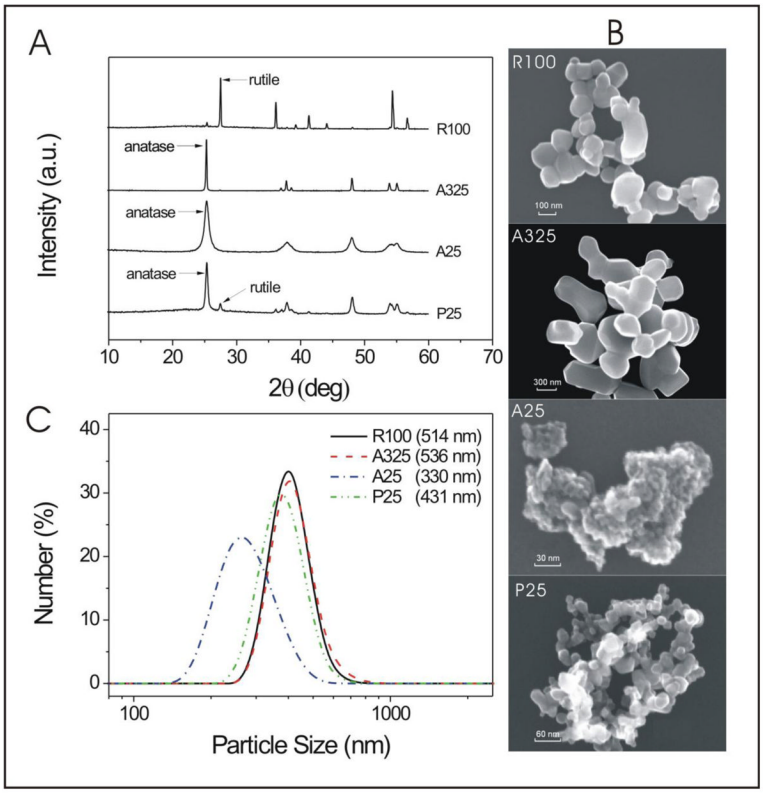

Figure 1. Characterization of Nano-TiO_2 samples. (A) XRD patterns of various TiO_2 samples; (B) SEM images of various TiO_2 samples; (C) **DLS determination of particle size and distribution of 50 μg/ml nano-TiO_2 samples in DMEM medium (FBS free).**

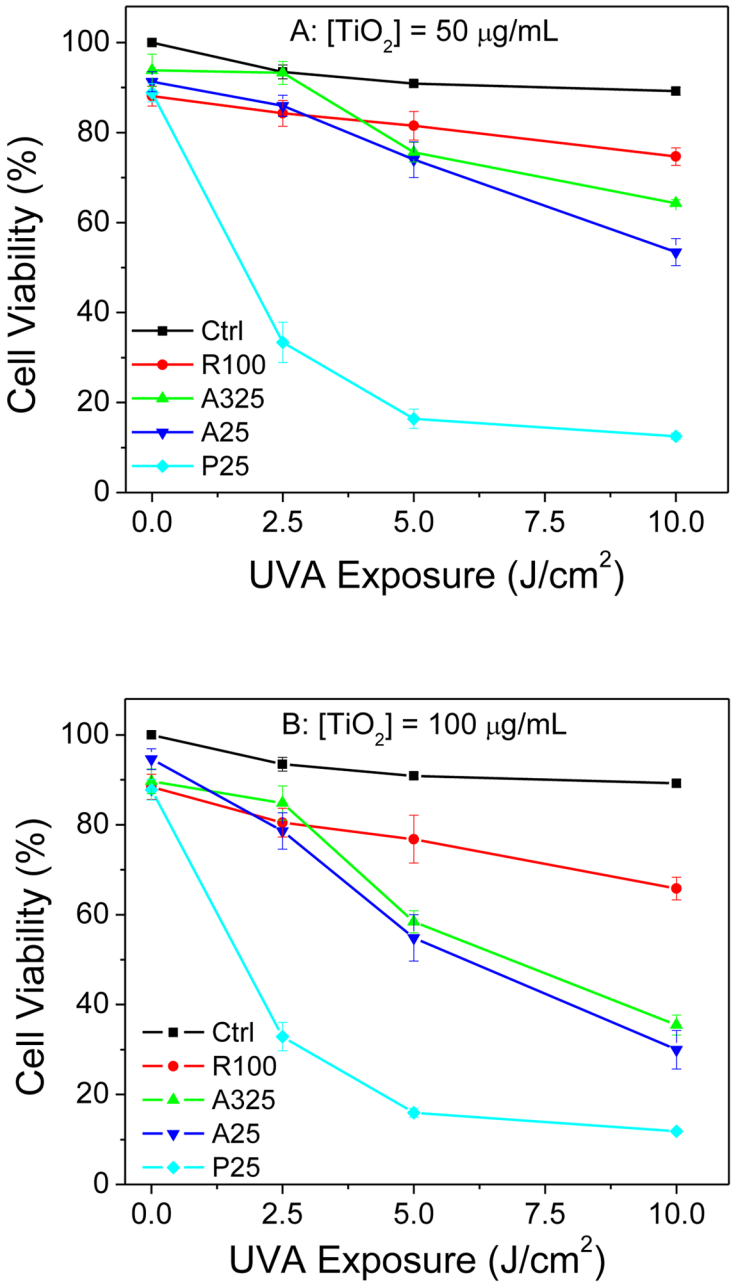

Figure 2.

Effect of exposure to different TiO_2 samples on the metabolic activity of HaCaT cells at concentrations of (A) 50 μg/ml and (B) 100 μg/ml as a function of UVA irradiation dosage, as measured by the MTS assay. Values are the means ± SE (n = 4).

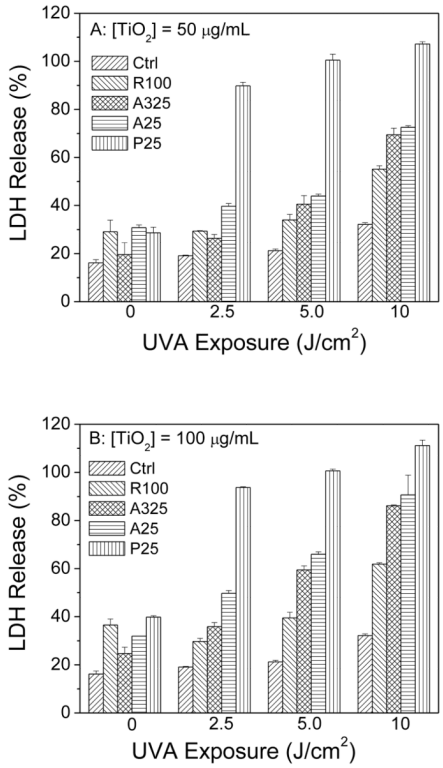

Figure 3.

Effect of exposure to different TiO_2 samples on the metabolic activity of HaCaT cells at concentrations of (A) 50 μg/ml and (B) 100 μg/ml as a function of UVA irradiation dosage, as measured by the LDH assay. Values are the means ± SE (n = 4).

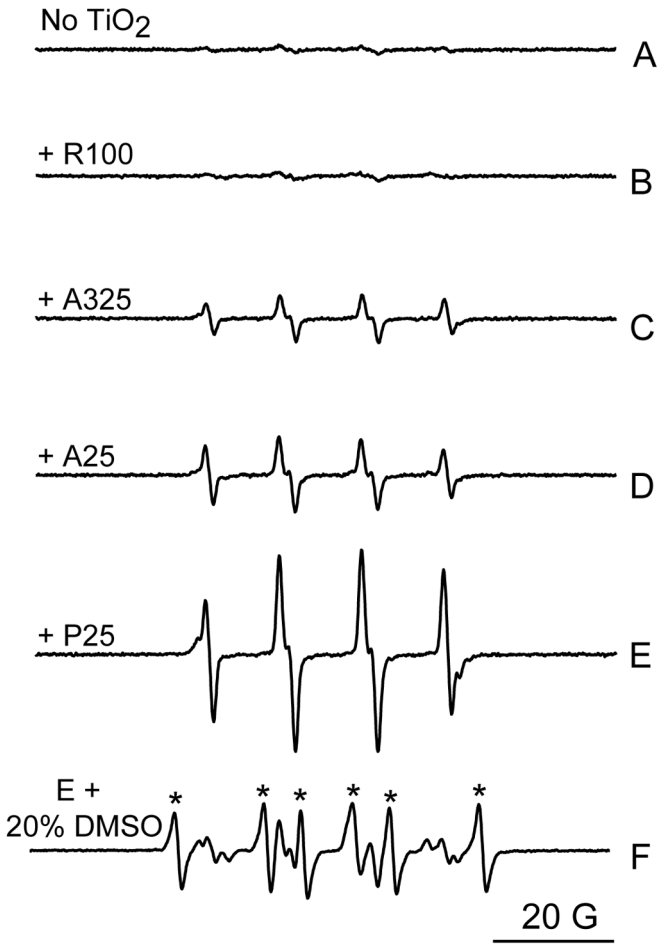

Figure 4.

Generation of hydroxyl radical from photoirradiation of TiO_2 samples under UVA light (340 nm). ESR spectra were recorded at room temperature 2 min after the UV light was turned on. Samples containing 25 mM BMPO and (A) without TiO_2; (B) with 0.1 mg/ml R100; (C) 0.1 mg/ml A325; (D) 0.1 mg/ml A25; (E) 0.1 mg/ml P25 and **(F) same as E, but with the addition of 20% DMSO. Stars (*) indicate the ESR signal of the BMPO/$^{\bullet}CH_3$ adduct.** Instrumental settings: microwave power, 10 mW; modulation frequency, 100 kHz; modulation amplitude, 1 G; scan range, 100 G.

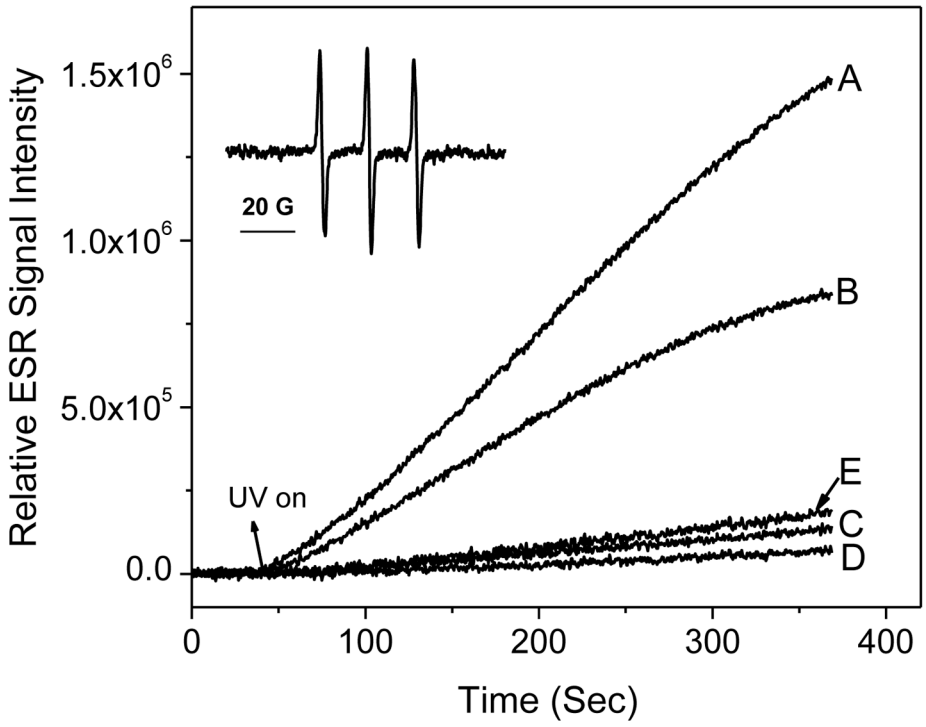

Figure 5.

Generation of singlet oxygen from photoirradiation of TiO_2 samples under UVA light in a time- and crystal type-dependent manner. ESR spectra were recorded at room temperature. Samples containing 20 mM TEMP and (A) 0.1 mg/ml P25, (B) 0.1 mg/ml A25 (C) 0.1 mg/ml A325, (D) 0.1 mg/ml R100, and (E) 0.1 mg/ml P25 and 10 mM NaN_3 were irradiated with UVA light at 340 nm. Inset: ESR signal of **TEMPONE** (a_N = 16.0 G). The time scans of ESR signal intensity were obtained with a fixed field position (the peak position of the center line of the ESR spectrum), 15 mW microwave power and 1 G field modulation.

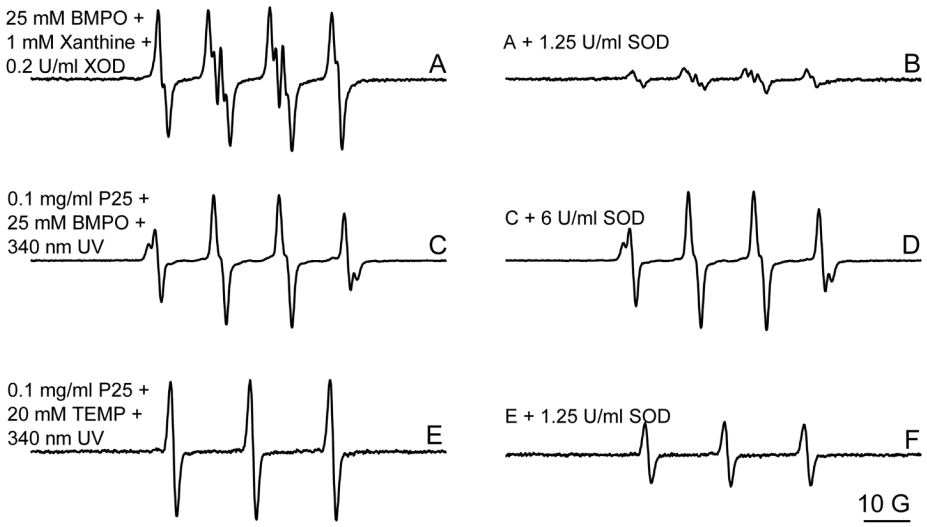

Figure 6.

Effect of SOD on the generation of hydroxyl radicals and singlet oxygen by P25 during UVA irradiation. The same conditions were used as shown in Fig. 4 and Fig. 5.

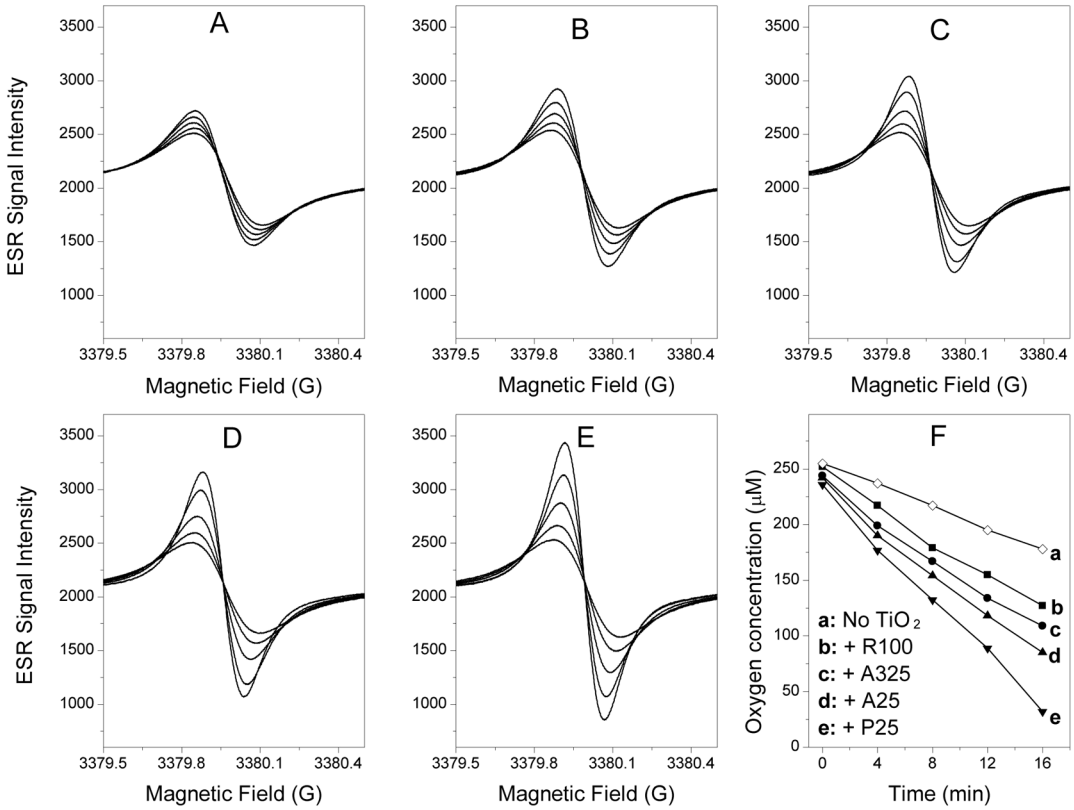

Figure 7.

Effect of TiO_2 samples on lipid peroxidation in liposomes. Oxygen consumption was measured in a closed chamber using liposome suspensions and the spin label ^{15}N-PDT. The liposome sample contained 30 mg/ml Egg PC and 0.1 mμ ^{15}N-PDT spin label mixed with (A) no TiO_2; (B) 0.03 mg/ml of R100; (C) 0.03 mg/ml of A325; (D) 0.03 mg/ml of A25 and (E) 0.03 mg/ml of P25. Lipid peroxidation was initiated by UV (340 nm) irradiation. The ESR spectra were recorded with the low field line of the ^{15}N-PDT spin label every 4 min after the sample was sealed in a quartz capillary tube. The spectra were obtained with 0.5 mW incident microwave power and with 0.05 G field modulation at ambient temperature. The progressive increases in peak-to-peak signal intensity (and accompanying progressive narrowing of the linewidth) in each panel are due to time-dependent oxygen consumption resulting from lipid peroxidation, **as shown in panel F**. The enhancement effects of different TiO_2 nanoparticles on lipid peroxidation may be seen as bigger changes in the peak-to-peak signal intensities seen in panels B, C, D and E compared to panel A.

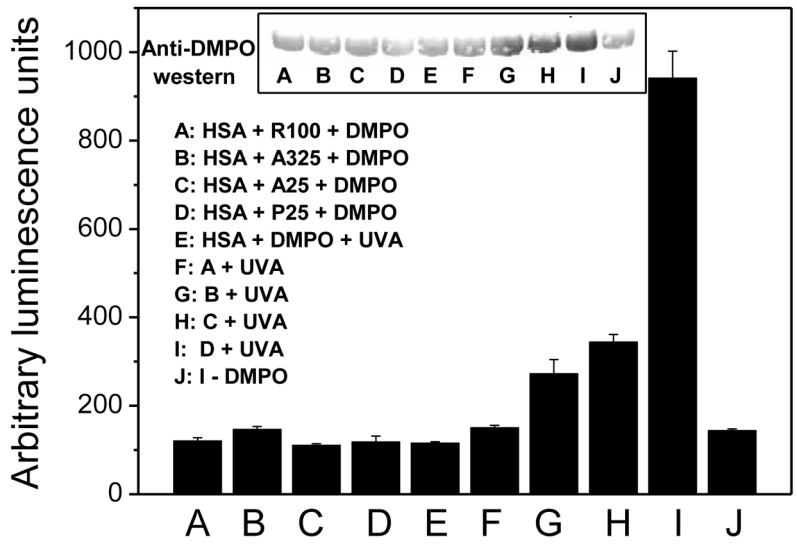

Figure 8.

Effect of TiO_2 samples and UVA irradiation on the formation of DMPO-HAS-derived radical nitrone adducts. Relative ELISA quantification and Western Blot analysis (inset).

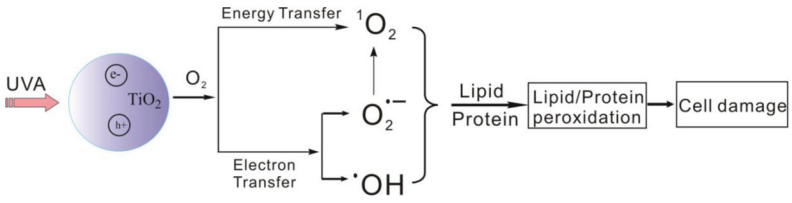

Figure 9.
Proposed mechanism of TiO_2 nanoparticle-induced free radicals and lipid/protein peroxidation leading to cell damage.